Fluorescence exclusion: a rapid, accurate and powerful method for measuring yeast cell volume

Daniel García-Ruano[1], Akanksha Jain[1], Joseph C. Ryan[1], Vasanthakrishnan Radhakrishnan Balasubramaniam[1], Larisa Venkova[2], Matthieu Piel[2] and Damien Coudreuse[1,*]

[1] Institute of Genetics and Development of Rennes, UMR 6290, CNRS – University of Rennes 1, France

[2] Institut Curie and Institut Pierre Gilles de Gennes, PSL Research University, CNRS UMR 144, Paris, France.

[*] Corresponding author: damien.coudreuse@univ-rennes1.fr

SUMMARY STATEMENT

Fluorescence exclusion provides a unique method to accurately measure the volume of yeast cells at both the population and single-cell levels.

ABSTRACT

Cells exist in an astonishing range of volumes across and within species. However, our understanding of cell size control remains limited, due in large part to the challenges associated with accurate determination of cell volume. Much of our comprehension of size regulation derives from models such as budding and fission yeast, but even for these morphologically stereotypical cells, assessment of cell volume has relied on proxies and extrapolations from two-dimensional measurements. Recently, the fluorescence exclusion method (FXm) was developed to evaluate the size of mammalian cells, but whether it could be applied to smaller cells remained unknown. Using specifically designed microfluidic chips and an improved data analysis pipeline, we show here that FXm reliably detects subtle difference in the volume of fission yeast cells, even for those with altered shapes. Moreover, it allows for the monitoring of dynamic volume changes at the single-cell level with high time resolution. Collectively, our work reveals how coupling FXm with yeast genetics will bring new insights into the complex biology of cell growth.

KEYWORDS

Cell volume, yeast, fluorescence exclusion

RUNNING TITLE

Measuring yeast cell volume

INTRODUCTION

Cell volume is a dynamic and complex trait that is modulated by both genetic and environmental components (Amodeo and Skotheim, 2016; Cook and Tyers, 2007; Lloyd, 2013; Marshall et al., 2012; Mueller, 2015). It has an impact on a host of cellular processes (Pedersen et al., 2001; Zhurinsky et al., 2010), playing important roles in tissue architecture and contributing to the overall size and shape of an organism (Amodeo and Skotheim, 2016; Cook and Tyers, 2007; Lloyd, 2013; Marshall et al., 2012; Mueller, 2015). At the single-cell level, volume and surface area not only define how cells sense external stimuli and interact with their environment but also determine their intracellular chemistry and organization. Strikingly, deregulation of cell size has dramatic consequences and is a hallmark of aging and cancer (Li et al., 2015; Pietras, 2011; Yang et al., 2011).

In proliferating cells, volume is intimately linked to the control of cell cycle progression. The dynamics of cell growth are complex across species, and specific stages of the cell cycle are associated with differential changes in cell size and morphology. For instance, while cells of the fission yeast *Schizosaccharomyces pombe* stop growing and maintain their overall shape during mitosis, mammalian cells undergoing division show a transient phase of rounding and volume alteration (Lancaster et al., 2013; Zlotek-Zlotkiewicz et al., 2015). In addition, size thresholds have been proposed to act as key checkpoints during the fission yeast cell cycle, allowing for the coordination of growth and division (Fantes, 1977; Fantes and Nurse, 1978; Fantes and Nurse, 1977). These mechanisms reduce cell-to-cell heterogeneity, thereby maintaining size homeostasis in a growing population.

Alterations in cell size are also triggered by changes in the environment, such as upon modulation of nutritional conditions, and cell cycle exit is often associated with a decrease in cell volume. For example, yeast cells exposed to nitrogen or glucose starvation enter quiescence with a significantly reduced size (Sun and Gresham, 2021). Interestingly, increases in cell volume were frequently observed during long-term experimental evolution in bacteria and were proposed to contribute to improved proliferation (Grant et al., 2021; Lenski and Travisano, 1994; Mongold and Lenski, 1996). This highlights how the volume of dividing cells may result from the necessary balance between growth advantages and evolutionary trade-offs.

The principles and mechanisms underlying cell size control have been the focus of in-depth investigation. While several pathways have been described to play a role in regulating this critical parameter (Amodeo and Skotheim, 2016; Cook and Tyers, 2007; Lloyd, 2013; Marshall et al., 2012; Mueller, 2015), whether they represent the key mechanisms that ensure size homeostasis remains unclear. Furthermore, how cells measure and control their geometric characteristics is surprisingly poorly understood. As a result, multiple models that are not mutually exclusive have been proposed: cells may divide 1) when they have reached a specific size (sizer), 2) after a specific time following a landmark cell cycle event (timer) and 3) after having produced a fixed amount of mass, at a rate that

depends on birth size (adder). While these possibilities are supported by experimental and theoretical studies (Fantes and Nurse, 1977; Mueller, 2015; Soifer et al., 2016; Sveiczer et al., 1996; Taheri-Araghi et al., 2015), general conclusions are difficult to draw. This may be due in part to the diversity of measurements used to describe cell size, including volume, surface area, cell length or dry mass. Indeed, the question remains whether one or a combination of these characteristics is more relevant for understanding size regulation and whether different cell types rely on the same or on distinct parameters. Thus, while the sizes and shapes of individual cell types are commonly accepted as fundamental hallmarks of cell identity, no unifying principles for size control have emerged.

Experimentally, the regulation of cell size has been difficult to investigate. In mammalian cell lines, the challenges of advanced genetic manipulation and the lack of simple methods for accurate measurement of parameters such as volume and surface area have been an obstacle to studying the molecular mechanisms of size control. Therefore, unicellular eukaryotes such as the budding and fission yeasts remain the models of choice for deciphering the bases of this critical cellular feature. In these organisms, regulation of cell size is intimately linked to the operation of the cell cycle machinery. Different concepts have thus emerged that may provide robust ways of regulating size, including titration mechanisms and dependence on geometric parameters (*e.g.* length, surface area) (Amodeo and Skotheim, 2016; Facchetti et al., 2019). However, how cells monitor their dimensions and how variation from the target size triggers a corrective response are not fully understood.

In the fission yeast *S. pombe*, the existence of cell size checkpoints was initially suggested at both S phase and, more importantly, mitosis (Fantes, 1977; Fantes and Nurse, 1978; Fantes and Nurse, 1977). While a mechanism based on an intracellular gradient of a cell cycle regulator was subsequently proposed (Martin and Berthelot-Grosjean, 2009; Moseley et al., 2009), recent evidence has challenged this model (Amodeo and Skotheim, 2016; Pan et al., 2014a; Saunders et al., 2012). Moreover, the commonly-employed approach of using cell length at division as a proxy for size may not be sufficient for investigating size regulation. First, cell volume is more critical to cell biology and biochemistry than length. Second, slight changes in the diameter of these rod-shaped cells are usually ignored, although they have a stronger impact on cell volume than similar alterations in length: the volume of a cylinder is linearly dependent on its length but varies with the square of its radius. In addition, morphology mutants or cells grown in conditions that induce alteration of cellular dimensions and scaling are complex to study and to compare with reference strains using this method. Finally, size at division restricts the analysis to only a small fraction of a proliferating population.

To investigate the control of yeast cell volume in a more unbiased manner, different techniques have been applied. These include volume calculation from geometrical assumptions, 2D imaging data that allow for 3D reconstruction or the integration of cellular sections extrapolated from the cell outlines, and complex approaches using advanced micromechanical devices (Baybay et al., 2020; Bryan et al., 2010; Bryan et al., 2014; Facchetti et al., 2019; Model, 2018; Pan et al., 2014b; Zegman et al.,

2015). However, these strategies are either low-throughput, difficult to establish or rely on various assumptions and complex processing of 2D measurements. For instance, given the impact of cell diameter on cell volume, accurate evaluation of cell size based on automated recognition of cell outlines requires this detection to be highly precise (Baybay et al., 2020; Zegman et al., 2015). Therefore, while these methods represent important steps in our capacity to address the regulation of cell volume, a more direct and simple methodology that does not introduce the biases of 2D data analysis or multiple steps of image segmentation and reconstruction is necessary.

Recently, a fluorescence exclusion method (FXm) was developed for evaluating the volume of morphologically diverse mammalian cells (Cadart et al., 2017). FXm relies on microfluidic devices in which cells are imaged in the presence of a fluorescently-labelled dextran that does not cross the plasma membrane. Thus, using chambers of known height, the local reduction in fluorescence due to the presence of a cell allows for the determination of the volume of this cell with high accuracy (Fig. 1A). This technique is simple and only requires single-plane imaging with low magnification objectives. It is unaffected by morphological alterations and is compatible with the monitoring of high numbers of cells. Although perfectly adapted to large mammalian cells, whether this new approach could be used for smaller cells such as yeast remained unclear, as this would require microdevices with significantly lower internal chambers. For example, HeLa cells are around 20-40 µm in height with a volume of ~1500 μm^3 at birth and ~3000 μm^3 at division (Cadart et al., 2018; Cadart et al., 2019). In contrast, wild-type fission yeast cells divide at a length of ~14 µm, with a diameter of ~4-4.5 µm. Depending on the growth conditions and exact diameter used for volume calculations, this led to values for size at division between ~120 and 200 μm^3 (Navarro and Nurse, 2012; Nurse, 1975).

Here we use the fission yeast *Schizosaccharomyces pombe* as a model system and demonstrate that the fluorescence exclusion method is a unique tool for measuring the volume of small cells. We engineer specific microdevices for yeast cells, assess the reproducibility and sensitivity of the system, and provide an improved way to perform large-scale analyses. Furthermore, we demonstrate the compatibility of the approach with multi-color imaging for evaluating single-cell volume in specific subpopulations. We then show how time-lapse experiments using these devices is a powerful strategy to couple yeast genetics with volume measurements for deciphering growth dynamics and size modulation. Interestingly, our results suggest that the use of FXm to re-evaluate previous models will be essential for understanding how cell volume is regulated in fission yeast, with implications for the general principles that govern cell size control in complex eukaryotes.

158 **RESULTS**

159 **Microfluidic devices for determining yeast cell volume by FXm**

160 FXm was developed to measure the volume of mammalian cells despite their complex
161 morphologies (Cadart et al., 2017; Cadart et al., 2018). This method is simple and potentially compatible
162 with any cell type, making it an ideal approach for investigating the regulation of cell volume in
163 genetically amenable models such as yeast. However, to ensure an optimal dynamic range for accurate
164 volume measurements, the height of the microfluidic chamber must be of the same order of magnitude
165 as that of the cells. Indeed, the exclusion of fluorescent molecules in a microsystem several times higher
166 than the cell would only marginally impact the total fluorescence intensity in the region of interest,
167 affecting the reliability of the results. Microdevices employed to determine mammalian cell volume are
168 therefore not adapted to small fission yeast cells, which require chambers of ~4-7 µm in height,
169 depending on the strain studied. Interestingly, evaluation of FXm suggests that such reduced heights
170 represent an advantage for the accuracy of these measurements (Model, 2020).

171 This design constraint led us to build specific and optimized devices for our yeast model. In
172 particular, we determined a density of normalization pillars that is high enough to prevent the collapse
173 of the chambers without significantly reducing the throughput of the method. Indeed, cells in close
174 vicinity of these pillars are excluded from the FXm analyses due to the bias introduced by the presence
175 of neighboring structures (Cadart et al., 2017). For this, we tested chambers with inter-pillar distances
176 of 120, 180 and 270 µm (Fig. 1B). We found a distance of 180 µm between pillars coupled with an
177 optimized cell concentration and preparation procedure to be the most reliable combination for the
178 measurement of high numbers of individual cells in a single frame while limiting cell aggregation (Fig.
179 1C, see Materials and Methods).

180

181 **Measuring the volume of individual fission yeast cells using FXm**

182 The necessity of using microchips of reduced height may represent a challenge for precisely
183 measuring the volume of individual yeast cells. Indeed, in these conditions, the difference between the
184 minimum (pillar) and maximum (no cell) fluorescence intensities (Fig. 1A), as well as the extent of
185 fluorescent molecule displacement in the presence of a cell, are inherently low. This may render the
186 technique less sensitive and more susceptible to noise, with consequences for its accuracy and
187 reproducibility.

188 To evaluate whether FXm provides high quality results for yeast, we measured the size of wild-
189 type fission yeast cells, comparing both the median volumes and volume distributions from independent
190 experiments (see Materials and Methods). To this end, we used a 5.53 µm high chamber design and
191 analyzed five replicates performed in separate devices built from the same master mold. Remarkably,

192 we obtained highly reproducible data, with a median volume for the pooled datasets of 104.8 ± 24.5
193 μm^3 (standard error for the 5 replicates, s.e.m.: 1.7 μm^3), and comparable population profiles (Fig. 2A).
194 This value for wild-type cells is consistent with previous results established by complex image
195 processing (Baybay et al., 2020), validating FXm for cell size monitoring in yeast. In contrast to size at
196 division, which only focuses on a small subpopulation, our method describes the volumes of the cells
197 over the entire population, from birth to division. It therefore integrates the changes in size that occur
198 during the division cycle. In addition, our experiments suggest that several repeats may be needed when
199 evaluating median volume differences of less than 10 %, as such alterations are in the range of the
200 observed experimental variability (Fig. 2A). When considering a geometric cell model consisting of a
201 cylinder with half spheres at both ends and a constant diameter of 4 µm, an increase of 10 % in volume
202 at division is the result of an increase in cell length at division from 14 to ~15 µm. Conversely, a similar
203 change in cell volume at constant length is brought about by an increase in diameter of ~0.2 µm. In both
204 cases, these differences are at the limit or below the resolution of the strategies routinely used for
205 measuring cell length or width in *S. pombe*. This demonstrates the high sensitivity of FXm for yeast
206 cell volume measurement, even when applying a conservative threshold of 10 % change.

207 Next, as molds deteriorate when heavily used and given that standard microfabrication procedures
208 make it difficult to generate highly reproducible chamber heights, we set out to evaluate how changes
209 in the dimensions of the devices may impact volume determination. We therefore produced microchips
210 of various heights and measured the size of wild-type fission yeast cells by FXm. Again, we observed
211 remarkably similar median volumes and volume distributions between measurements (Fig. 2B – median
212 volume of the pooled datasets: 106.8 ± 24.4 μm^3; s.e.m. for the 5 replicates: 1.9 μm^3). This shows that
213 data obtained with different devices can be reliably compared.

214 Finally, we further validated the approach by assessing the volumes of known fission yeast size
215 mutants as well as wild-type diploid cells. In particular, we measured the size of well-described
216 temperature-sensitive cell cycle mutants: *wee1-50*^{ts} (small cells) and *cdc25-22*^{ts} (large cells) (Fantes,
217 1979; Fantes and Nurse, 1978; Nurse, 1975). As anticipated, *wee1-50*^{ts} and *cdc25-22*^{ts} cells grown at
218 the permissive temperature of 25 °C showed significantly smaller and larger volumes than wild type,
219 respectively (Fig. 2C, Fig. S1A). Note that the apparent broader distribution in *cdc25-22*^{ts} results from
220 increased overall size, as the volume profiles of these strains are similar when the data are normalized
221 to their respective median sizes (Fig. S1C). In the case of wild-type diploid cells, we found that the
222 median population volume is 1.84-fold higher than for haploid cells (Fig. 2D, Fig. S1B).

223 Altogether, these experiments demonstrate that FXm with specifically adapted microfluidic chips
224 is compatible with the analysis of yeast cell volume and produces highly reproducible results.
225 Furthermore, in contrast to measurements of cell length and width, FXm does not rely on 2D parameters
226 that are difficult to accurately determine. In particular, it will allow for identifying changes in volume

227 that result from limited alterations in cell diameter. Finally, our data also set a first conservative
228 threshold of 10 % for the estimation of differences in cell volume between populations.

229

230 **Improving FXm image analysis**

231 FXm image analysis consists of three steps (Cadart et al., 2017): image normalization, cell
232 selection and volume calculation. However, as FXm requires a low magnification objective, the size of
233 yeast cells and the high number of cells in a frame make it tedious to manually select individual cells
234 using the code established for mammalian cells. Interestingly, the normalization procedure generates a
235 mask that separates pillars and cells from the background (Cadart et al., 2017). Since the majority of
236 objects extracted at this step corresponds to valid individual cells, we took advantage of this mask and
237 developed a Python script to assist the user in cell selection (see Supplementary information). Thus,
238 instead of manually delineating the multiple regions of interest (Fig. 3A), this tool offers two distinct
239 strategies.

240 First, a manual cell selection mode can be chosen. Cells pre-selected by the normalization mask
241 are magnified and displayed (Fig. 3A), allowing the user to rapidly exclude incorrect objects such as
242 dust particles or cell aggregates. This approach makes the analysis of a high number of cells easier and
243 faster. Second, an automated and non-discriminatory selection can be applied. To exclude aberrant
244 measurements (*e.g.* cell aggregates, small dead cells), thresholds are then automatically set to remove
245 outliers based on the standard deviation (s.d.) of the population data. This is more appropriate than the
246 use of absolute cut-offs, which may need to be adjusted from strain to strain. After testing different s.d.
247 thresholds (data not shown), we found that excluding values outside of 2 s.d. (1 IQR for a normal
248 distribution) for the first and third quartiles was optimal for obtaining results similar to those established
249 with the manual method, correctly selecting between 87 and 92 % of the objects in our experiments
250 (Fig. 3B). Finally, our script also provides the option of separating the selected cells in different groups.
251 This is particularly useful when determining the volumes of distinct subpopulations, for instance based
252 on additional fluorescence markers (see below).

253 Collectively, the improvements brought by our analysis code facilitate FXm and provide more
254 options to the user for complex studies of cell populations. Interestingly, while manual selection is the
255 most accurate approach, we show that automated analysis with outlier exclusion allows a rapid
256 assessment of high numbers of cells while remaining sufficiently reliable for screening the volumes of
257 many different strains.

258

259

260

261 **Small variations in cell dimensions and population heterogeneity**

262 Our initial volume measurements in wild-type fission yeast cells and the evaluation of FXm
263 experimental variability suggest that changes in volume ≥10 % can be reliably detected (Fig. 2). To
264 further assess the sensitivity of FXm, we first determined the volume of cells showing a marginal
265 difference in length at division compared to wild type. To this end, we took advantage of a fission yeast
266 strain whose proliferation relies on a minimal cell cycle control network (MCN). In this background,
267 cell proliferation is solely dependent on the oscillation of a single cyclin-dependent kinase (CDK)
268 activity between two thresholds (high for mitosis and low for S phase) (Coudreuse and Nurse, 2010).
269 This is achieved through the expression of a fusion protein between cyclin B/Cdc13 and Cdk1/Cdc2, in
270 the absence of all other cell cycle cyclins (Coudreuse and Nurse, 2010). Interestingly, while behaving
271 similarly to wild type (Coudreuse and Nurse, 2010), MCN cells show a minor increase of ~7 % in their
272 length at division in our experimental conditions (15 µm for wild type and 16.1 µm for MCN cells, Fig.
273 4A). This is predicted to contribute to a similar increase in volume according to the geometric model of
274 *S. pombe* cells (see above). Unexpectedly, FXm measurements showed a median volume difference of
275 17 % between these strains (Fig. 4A, Fig. S2; compare WT and MCN). This suggests that the change
276 in size between wild type and MCN cells is not solely the result of an increase in cell length.
277 Importantly, it demonstrates that FXm is a promising approach for investigating volume regulation in
278 yeast, providing novel and more in-depth information on cell size and geometry.

279 Next, we tested whether FXm can reliably reveal volume changes below our initial threshold of
280 10 %. First, building on the results in Fig. 2A and 2C, we showed that a difference in volume of less
281 than 10 % between wild-type cells grown at 32 *vs*. 25 ºC could be robustly established by simply
282 increasing the number of experimental replicates (Fig. 4B and Fig. S3A). We then investigated whether
283 even smaller alterations in volume at the population level could be detected as cells progressively
284 change size over time. As a proof-of-concept, we used MCN cells, as they harbor a mutation in the
285 Cdc2 moiety of the fusion module that makes them sensitive to dose-dependent and reversible inhibition
286 of CDK activity by non-hydrolysable ATP analogues such as 3-MBPP1 (Bishop et al., 2000; Coudreuse
287 and Nurse, 2010). This allowed us to block cells in G2 using the inhibitor, let them synchronously re-
288 enter the cell cycle upon inhibitor wash-off (Fig. S3B, C) and monitor volume changes throughout the
289 following G2 with high time resolution (Fig. 4C). Remarkably, even considering the experimental
290 variability observed at certain time points, very small increases in volume (<5%) and changes in growth
291 rates could be measured, demonstrating the high sensitivity of FXm in this context.

292 Another critical parameter in our understanding of cell size homeostasis is the size distribution in
293 the population. This reflects the cell-to-cell heterogeneity in cell cycle progression and the strength of
294 the size control operating in these cells. To date, most studies in fission yeast have focused on variability
295 in cell length at division. However, not only does this approach exclude the majority of cells, but our
296 results above suggest that evaluating cell volume distribution may lead to different conclusions. To

297 establish whether FXm is sufficiently sensitive for monitoring alteration of cell size profiles, we took
298 advantage of MCN cells in which the target residues of the conserved Wee1/Cdc25 feedback loop on
299 Cdc2 are mutated (T14A Y15F, MCN-AF) (Coudreuse and Nurse, 2010). Loss of this mitotic switch
300 results in an increase in cell-to-cell variability in length at division (Coudreuse and Nurse, 2010). In the
301 non-supplemented medium used in our experiments, we also found that these cells are on average
302 slightly smaller than wild type (Fig. 4A). As anticipated, we observed a broader distribution of cell
303 volume in MCN-AF compared to MCN and wild-type cells (Fig. 4A, D). Interestingly, the relative
304 changes in median volume *vs.* average length at division between MCN-AF, MCN and wild type
305 provide insights into the dimensions that are altered in these strains. (Fig. 4A, Table S1): while MCN-
306 AF and MCN appear to differ only in length (same ratios for volume *vs.* size at division), both strains
307 are likely to show an increase in cell diameter compared to wild type (differing ratios).

308 Altogether, these results demonstrate that FXm is easier and more sensitive than previously used
309 methods, enabling the monitoring of small alterations in cell volume and changes in size homeostasis
310 in populations of yeast cells. Coupling these data with more traditional cell length measurements will
311 shed light on how changes in volume are mediated and whether modulations of cellular geometry occur.

312

313 **Measuring the size of cells with altered geometries and morphologies**

314 FXm allows for measuring small changes in size that are difficult to accurately evaluate from cell
315 length and diameter measurements. The use of length as a proxy for fission yeast size is even more
316 problematic when studying mutants or conditions where dimension scaling or cell shape is altered.
317 Furthermore, strategies using cell outline detection to extrapolate cell volume may not be sufficiently
318 reliable, given the influence of minor changes in diameter on cell volume.

319 In this context, we determined the volumes of various strains showing defects in morphology and
320 shape. First, we assessed the size of strains lacking Rga2, Rga4 or Rga6, which are members of the
321 RhoGAP family. These factors are involved in polarized growth, and their loss impacts cell geometry
322 (Das et al., 2007; Revilla-Guarinos et al., 2016; Soto et al., 2010; Villar-Tajadura et al., 2008). When
323 ranking these strains according to their length at division, we found that Δ*rga2* cells are the longest,
324 followed by Δ*rga6* and Δ*rga4* (Fig. 5A). Strikingly, FXm, which is unaffected by changes in either
325 morphology or geometry, led to the opposite conclusion, with Δ*rga4* and Δ*rga2* cells having the largest
326 and smallest volumes, respectively (Fig. 5B, Fig. S4). This shows that cell length measurement is not
327 reliable as a proxy for cell size when studying such mutants. Our data also demonstrate the advantages
328 of FXm for establishing size differences between strains and determining the influence of diverse
329 pathways on cell volume regulation.

330 Next, we used FXm to evaluate the size of cells for which length can be difficult to measure or
331 inherently inaccurate due to morphological alterations. To this end, we used bent cells *(Δknk1, Δtea1)*

332 as well as cells with significant shape defects and irregular diameters (Δ*mal3*) (Beinhauer et al., 1997;
333 Mata and Nurse, 1997; Scheffler et al., 2014) (Fig. 5C). As anticipated, while cell length at division
334 could not be determined without excluding a significant fraction of the cells, FXm allowed us to
335 establish the profiles of cell volume in these populations and compare them with that of wild-type cells.
336 This again highlights the power of this method for studying size control mechanisms independently of
337 cell morphology (Fig. 5D, Fig. S5). Interestingly, in cells with morphological defects, both the median
338 volume and size distribution may change (Figs. S4, S5), potentially reflecting alterations of their cell
339 cycle organization and associated growth patterns. This opens the door to investigating how cell shape
340 may delineate the complex interplay between cell growth and the division cycle at the single-cell level.

341 Finally, we evaluated FXm data for significantly smaller cells that have stopped dividing. Upon
342 glucose exhaustion, fission yeast cells exit the cell cycle and enter a non-proliferative quiescent state,
343 which is associated with a dramatic reduction in cell size. Given the shape of the cells in these conditions
344 (Fig. 5E), determining their length and width to extrapolate their volume is difficult and unreliable. In
345 contrast, FXm established high-quality profiles of cell volume in these populations (Fig. 5F, Fig. S6).
346 This will allow for investigating the impact of cell size on cell physiology and aging in this critical
347 cellular state.

348 Collectively, this set of experiments demonstrates the versatility of FXm, which provides an
349 unprecedented ability to measure the size of any strain, irrespective of cell morphology and
350 physiological status. Our results also suggest that previous conclusions on size control in fission yeast
351 may need to be re-evaluated using FXm.

352

353 **Measuring the volume of subpopulations**

354 All experiments presented so far focus on the determination of cell volume in entire cell
355 populations. However, extracting the size of cells in specific subpopulations is critical for understanding
356 how different biological processes may interact with the mechanisms underlying cell size control and
357 how cell growth and proliferation are coupled. Thus, associating FXm with the use of other intracellular
358 fluorescent markers would represent a powerful method to take advantage of yeast genetics and explore
359 the complexity of size regulation in different conditions and throughout the cell cycle. Similarly, this
360 could allow for discriminating between distinct strains expressing specific markers in a complex
361 population, opening the door to exploring non-cell autonomous processes that may feed into volume
362 regulation.

363 To evaluate these approaches, we set out to determine cell volume at mitosis, using the non-histone
364 chromatin-associated protein Nhp6 coupled to the red fluorescent marker mCherry. First, we validated
365 that the presence of Nhp6::mCherry in the nucleus did not induce any significant signal in the FITC
366 channel under FXm conditions (Fig. S7A). This also showed that the slightly reduced volume of these

367 cells compared to wild type (Fig. 6A, Fig. S7B) results from an alteration of Nhp6 function due to the
368 tag rather than an experimental bias from mCherry fluorescence. Using our improved FXm code, we
369 segmented the population of binucleated cells (~11 % of the total number of cells) and determined their
370 median volume (126.3 ± 18.2 μm^3, compared to 93.5 ± 21.3 μm^3 for mononucleated cells, Fig. 6B). The
371 partial overlap between mono- and binucleated cells is consistent with the interruption of growth during
372 mitosis: cell size does not change throughout nuclear division, and growth only resumes in G1. Note
373 that the volume of binucleated cells measured in our assay is consistent with previous calculations of
374 cell volume at division (Nurse, 1975) but significantly differs from those presented in a more recent
375 study (Navarro and Nurse, 2012). This further demonstrates that fission yeast cell size cannot be reliably
376 and reproducibly determined using cell length and diameter. Altogether, our experiments validate the
377 possibility of combining FXm with additional markers in yeast for more complex investigations of cell
378 size control and dynamics.

379

380 **Dynamic changes in fission yeast cell volume at the population and single-cell levels**

381 Next, we tested the use of FXm for assessing dynamic changes in yeast cell size. First, we
382 ascertained whether coupling time course experiments with FXm allows for following induced
383 alterations in cell volume over time using asynchronous populations. A wide range of growth conditions
384 (*e.g.* heat stress (Vjestica et al., 2013), osmotic stress (Millar et al., 1995), change in nutrient availability
385 (Fantes and Nurse, 1977; Petersen, 2009)) as well as experimental modulation of specific cellular
386 pathways can trigger cell size changes. Understanding the dynamics of such changes may be key to
387 determining the implication of these processes in cell size homeostasis. To evaluate FXm in this context,
388 we took advantage of the analog-sensitivity of MCN cells. Indeed, reducing Cdc2/CDK activity in
389 fission yeast using this method leads to an increase in cell size (Chen et al., 2016; Coudreuse and Nurse,
390 2010). We therefore measured cell volume in asynchronous MCN cells at 40-minute intervals (~1/4 of
391 the cell cycle) after treatment with 0.05 µM 3-MBPP1 (Fig. 7). Our data show that MCN cells
392 progressively increase their volume, up to 1.7-fold after one doubling time. Strikingly, comparison of
393 the volume *vs*. size at division ratios throughout the experiment (Table S1) suggests complex dynamics
394 in the respective modulations of length and diameter upon CDK inhibition. This demonstrates that FXm
395 1) can be used to follow short-term alterations in median cell size and size distribution in asynchronous
396 yeast populations and 2) provides new perspectives for our understanding of how the geometrical
397 dimensions of these cells contribute to cell volume.

398 We then asked if FXm could be applied to analyze individual yeast cells in time-lapse experiments.
399 First, we determined the experimental noise for single cells in our chips by comparing 20 successive
400 measurements of 10 individual cells over a period of ~6 seconds (Fig. 8A). Making the assumption that
401 no volume changes occur in such a short time, this showed that the variability inherent to FXm when

402 using chips of reduced height remains very limited. Interestingly, it also suggests that when monitoring
403 single cells, volume alterations as low as ~3 % can be detected. Next, to perform time-lapse experiments
404 of several hours, we began by using modified chips in which the cell injection inlets were made bigger
405 (from 2.5 to 4 mm), acting as nutritional reservoirs to maintain growth conditions as stable as possible.
406 As fission yeast cells are non-adherent, this also required pre-coating of the chip coverslips with lectin.
407 In this context, we observed a linear increase in volume during each cell cycle and a plateau in size
408 around the time of cell division, corresponding to the well-described growth arrest at mitosis
409 (Mitchison, 1957; Mitchison and Nurse, 1985) (Fig. 8B). However, we found that in these experiments,
410 cells divide at smaller sizes in succeeding cell cycles, suggesting that the built-in reservoirs are
411 insufficient to ensure a favorable growth environment throughout our assay. We therefore applied a
412 constant flow of fresh medium containing FITC-Dextran (~3-5 $\mu L.min^{-1}$) for the entire duration of the
413 experiments. In this setup, we did not detect any consistent reduction in cell volume at division after
414 each cycle (Fig. 8C). Furthermore, in the presence of flow, the growth rate (see Materials and Methods)
415 was significantly higher than without medium renewal (Fig. 8B, C).

416 These data demonstrate that FXm is a unique tool for monitoring volume dynamics of small cells
417 with a high time resolution and for detecting changes in growth rate at the single-cell level. This will
418 allow for investigating the immediate responses of cells to environmental perturbations and the
419 behaviors of separate yeast cell lineages. In addition, this will make it possible to relate volume at birth,
420 growth rate and volume at division for a given cell. Coupled with additional markers, this technique
421 thus offers an unprecedented entry into the investigation of cell size control and its interplay with
422 complex biological processes.

423

424

425 **DISCUSSION**

426 Regulation of cell volume is critical for eukaryotic organisms, but the mechanisms underlying this
427 process are still unclear. Yeast models have played a pioneering role in deciphering this complex trait
428 and remain at the forefront of this very active research field. However, the difficulty of accurately
429 measuring cell volume in these small unicellular organisms has been an obstacle for our understanding
430 of size control and homeostasis. Here we show that the fluorescence exclusion method (FXm) is ideal
431 for evaluating the volume of small yeast cells in diverse contexts. It provides high quality data on the
432 volume profiles of yeast populations irrespective of cell morphology and physiological state, allows for
433 single-cell analysis of volume changes with high time resolution and is compatible with the use of
434 additional fluorescent markers. Our experiments also demonstrate that FXm gives researchers unique
435 access to in-depth analyses of yeast cell volume dynamics and their coupling with cell cycle
436 progression, integrating the size of cells at all stages of their division cycle. Furthermore, combining
437 FXm with time-lapse imaging represents an unprecedented tool for exploring the changes in growth
438 rate and cellular geometry that occur not only during proliferation or upon major transitions such as
439 quiescence entry and exit, but also when cells respond to acute challenges. Thus, we believe that this
440 technique will become a new standard for investigating cell size control in yeast, with implications for
441 our knowledge of size regulation in complex eukaryotes.

442 Interestingly, our work led to a number of observations that may question existing models of cell
443 size regulation. First, research on *S. pombe* size control and its interplay with cell cycle progression has
444 mostly been based on the assumption that the diameter of proliferating haploid fission yeast cells is 1)
445 constant from one cell to another and 2) homogenous along their growing axis. Our results clearly
446 indicate that these assumptions can lead to incorrect conclusions when comparing strains, as shown
447 using various mutants (Figs. 4, 5). In this context, FXm has the advantage of being a direct method for
448 volume measurement that does not rely on any pre-conceived idea of cell geometry. Coupling FXm
449 with cell length measurements also offers an additional level of understanding of cell size dynamics.
450 For example, our data suggest that when cells are arrested in their division cycle through CDK
451 inhibition, the geometric changes that occur over time are surprisingly complex, with length and volume
452 alterations showing different kinetics (Table S1, MCN + 3-MBPP1). Similarly, we find that simplifying
453 the architecture of cell cycle control or growing cells in distinct environments has unanticipated impacts
454 on cell geometry, affecting both cell length and diameter (Table S1).

455 Moreover, focusing on subpopulations, as is the case when using cell length at division as a proxy
456 for cell size, may hamper our comprehension of important processes linking cell growth, morphology
457 and proliferation. For instance, the apparent changes in size distribution at the population level in
458 morphology mutants suggest that the interplay between growth rate and cell cycle phases may be altered
459 in these cells. This again may shed light on potentially novel inputs and mechanisms that modulate cell
460 size dynamics. In this context, the different cell geometries of *rga* mutants (Table S1), as indicated by

our comparisons of volume *vs*. cell length at division ratios, may represent a promising model for uncovering the key parameters used by the cells to "monitor" their size.

Our work demonstrates that previous models that describe the way cell size is regulated in fission yeast need to be revisited using FXm. Together with the wealth of knowledge on size control in this organism, this approach will provide new insights into the processes that underlie the biology of cell growth. Interestingly, the investigation of biological processes has been enriched by the use of natural yeast isolates. In fission yeast, these strains are known to be less homogenous in morphology and overall size (Jeffares et al., 2015). FXm may therefore make it possible to fully exploit this unique resource and take advantage of advanced population genetics strategies to decipher the regulation of cell size. While we use fission yeast as a proof-of-concept model, our results also show that FXm can be applied to any type of cell over a broad range of sizes. Our studies therefore establish the versatility and power of FXm for investigating cell volume homeostasis and its regulation in small cells and model organisms, contributing to our general understanding of the modulation of cellular dimensions and scaling in eukaryotes.

476 **MATERIALS AND METHODS**

477 **Fission yeast strains and methods**

478 Standard methods and media were used (Hayles and Nurse, 1992; Moreno et al., 1991). All the strains
479 described in this study are detailed in Table S2. The deletions of *rga2*, *rga4*, *rga6*, *mal3*, *knk1* and *tea1*
480 have already been described (Soto et al., 2010; Villar-Tajadura et al., 2008) (Beinhauer et al., 1997;
481 Mata and Nurse, 1997; Revilla-Guarinos et al., 2016; Scheffler et al., 2014). All experiments were
482 carried out in non-supplemented minimal medium (EMM) at 32 ºC, except otherwise noted. To inhibit
483 CDK activity in analog-sensitive MCN strains, the 3-MBPP1 inhibitor (A602960, Toronto Research
484 Chemicals, Inc.) was dissolved in DMSO at stock concentrations of 10 or 0.4 mM and added to liquid
485 cultures at a final concentration of 1 or 0.05 µM. The percentage of binucleated cells (Fig. S3C) was
486 determined from heat fixed samples on microscope slides (70 ºC for 5 min) stained with a 11:1 solution
487 of Blankophor (1 mg/mL): DAPI (1 µg/mL).

488

489 **Microfabrication of FXm chips**

490 PDMS microfluidic chips for FXm were prepared following standard microfabrication protocols
491 (McDonald and Whitesides, 2002). In brief, master molds were made by spin-coating SU-8 2005 resin
492 (MicroChem Corp., USA) on silicon wafers using a spincoater (Laurell Technologies, USA) according
493 to manufacturer's instructions. Microstructures were then generated using high-resolution chrome
494 masks (JD phototools, UK) and 365nm UV exposure (UV KUB 3, Kloe, France) followed by PGMEA
495 (Sigma-Aldrich) development. For each mold, the height of the structures was determined as the
496 average of three measurements perpendicular to the long axis of the design (Fig. 1B) using a Veeco
497 Wyko NT9100 optical profilometer (Veeco Instruments Inc., USA). Note that molds showing
498 significant variability between the three height measurements should be either discarded or used
499 considering local rather than global averaged height. To produce chips for FXm, a 10:1 mixture of
500 PDMS (Sylgard 184, Dow Corning, USA) was cast on the SU-8 master mold and allowed to cure at 70
501 °C for 2 hours. Inlets were then made using 2.5 or 4 mm biopsy punches, and chips were bonded to
502 microscopy-grade coverslips by plasma activation (Harrick Plasma, USA).

503

504 **Preparation of fission yeast cells for FXm**

505 To perform FXm experiments, exponentially growing fission yeast cells were sampled at an optical
506 density between 0.25 and 0.45 OD_{595}. To limit the formation of cell aggregates, a mild sonication cycle
507 of 5 s at 10 % amplitude (Branson 450 Digital Sonifier, Emerson Electric Co.) was applied. This
508 treatment had no effect on the results we obtained by FXm (data not shown). In order to optimize the
509 number of cells that can be measured on a single FXm image in our chip design, cells were concentrated
510 to ~5.5×10^7 cells/mL in their own conditioned minimal medium (note that to prevent bias in our volume
511 measurements, we did not use autofluorescent rich medium). FITC-Dextran was then added to the

512 sample (FD10S, Sigma Aldrich) at a final concentration of 1 mg/mL, and cells were loaded into the
513 chip shortly before image acquisition. For evaluating the volume of quiescent cells, cells were sampled
514 24 hours after they reached 0.4 OD_{595}.
515
516 **Microscopy**
517 All microscopy experiments were carried out using an inverted Zeiss Axio Observer (Carl Zeiss
518 Microscopy LLC) equipped with a Lumencor Spectra X illumination system and an Orca Flash 4.0V2
519 sCMOS camera (Hamamatsu Photonics). Acquisition was performed using the VisiView software
520 (Visitron Systems GmbH). A Plan-Apochromat 63X/1.4 NA immersion lens and a Plan-Apochromat
521 20X/0.8 NA Ph2 lens (Carl Zeiss Microscopy LLC) were used for cell length measurements and FXm,
522 respectively. For routine volume measurements, the acquisition parameters were 100 ms exposure at 20
523 % illumination power, and 30 to 40 images were taken across the whole chambers to limit potential bias
524 due to local changes in chamber height. For the time-lapse experiments in Fig 8, 100 ms exposure at 10
525 % illumination power was used.
526
527 **Image analysis**
528 Cell length at division was determined from Blankophor images (1 mg/mL Blankophor solution,
529 A108741, Ambeed Inc.) using FIJI (National Institutes of Health) and the Pointpicker plug-in. For the
530 blankophor images in Fig. 2, 4, 5 and 7, the brightness and contrast were adjusted for display purposes.
531 For routine volume measurements, images were first normalized using a custom Matlab software
532 (Cadart et al., 2017). Cell selection and volume calculation were subsequently performed using the
533 normalization mask with a new, specifically-developed Python interface (see Results). For all Figures,
534 cell selection was done using the manual mode, except for Fig. 3B and 4C where automated cell
535 identification was used. Note that except for the time-lapses in Fig. 8B and C, we systematically
536 excluded cells that were undergoing cytokinesis but that had not fully separated into two individual
537 daughter cells; this is similar to studies of cell length at division. While this category can be integrated
538 as newly-born pairs of cells using the original Matlab software (Cadart et al., 2017), manually
539 delineating the division site would introduce measurement errors. Finally, our Python code is not
540 adapted to tracking the volume of individual cells in long time-lapse experiments (Fig. 8B, C), as slight
541 cell movements make it difficult to reliably follow single cells over time when using the normalization
542 mask pre-selection. For these assays, we used the original Matlab software (Cadart et al., 2017).
543
544 **FXm time-lapse and analysis using fission yeast**
545 As fission yeast cells are non-adherent, FXm time-lapses required coverslips to be coated in order to
546 prevent cells from moving inside the chamber, which would hamper data acquisition and analysis. To
547 this end, 10 µl of 1mg/ml filtered lectin was spread in a rectangle of ~10x5 mm at the center of the
548 coverslip and allowed to dry at 37 ºC. The coverslip was then washed once with filtered ultra-pure water

549 and dried at 37 ºC. For experiments without medium flow (Fig. 8B), Ø 4 mm inlets were made in the
550 PDMS chip using the appropriate biopsy punch. 5 µl of cells prepared as described above were loaded
551 in one inlet, and both inlets were then filled with 45 µl EMM containing the FITC-Dextran dye. Cells
552 were allowed to flow into the chamber prior to imaging. For time-lapse experiments using medium flow
553 (Fig. 8C), two successive layers of lectin were applied as above and inlets of Ø 0.75 mm were fabricated.
554 Cells were then loaded by depositing a drop of cells prepared as above over one of the inlets, and a mild
555 vacuum was applied at the other inlet using the tip of a 10 mL pipet connected to a vacuum pump. The
556 loaded chip was then connected to a flow control system (pressure generator and flow controller,
557 Elvesys, France), and a flow of medium (~3-5 µL/ min) containing the FITC-Dextran dye was used
558 throughout the experiment. For the analysis of the time-lapse experiments, the two daughter cells after
559 a division were manually delineated during the analysis and only one of them was followed for further
560 investigation (Fig. 8B, C). The growth rate of each individual cell was determined by calculating the
561 slopes of the traces during each cycle. This was obtained by linear regression considering the volume
562 at birth as the first time point (when an invagination is detected) and excluding the mitotic plateau: entry
563 into mitosis was assigned to the last point prior to strong reduction of growth (when two consecutive
564 points on the graph decrease the slope).
565
566
567 **ACKNOWLEDGMENTS**
568
569 We thank Pei-Yun Jenny Wu and Snezhana Oliferenko for critically reading the manuscript. We thank
570 Pascal Hersen and Giacomo Gropplero for the measurements of our chamber heights. We are grateful
571 to Paul Nurse, Snezhana Oliferenko, Pilar Perez and Phong Tran for sharing strains and reagents.
572
573
574 **COMPETING INTERESTS**
575
576 No competing interests declared.
577
578
579 **FUNDING**
580
581 This work was supported by a grant to DC from the Agence Nationale de la Recherche (ANR, project
582 eVOLve, ANR-18-CE13-0009; funding for AJ and DGR) and the Région Bretagne (ARED Pombevol,
583 funding for DGR). JCR was supported by a fellowship from the Ministère de l'Enseignement Supérieur
584 et de la Recherche. VRB was supported by an ERC Starting Grant to DC (SyntheCycle, Grant
585 Agreement no. 310849).

586 **FIGURE LEGENDS**

587 **Figure 1. Microfluidic chips for FXm. A.** Schematic of the principles of FXm (Cadart et al., 2017).
588 Left: cells are injected in a FXm chip (see *B*) in the presence of FITC-Dextran. Pillars are integrated for
589 ceiling support and image normalization. A low-magnification objective is used to acquire single-plane
590 images (see *C*). Right: After normalization, the volume of the cell can be determined from the loss of
591 fluorescence (grey area, the precise internal height of the chip must be determined (Cadart et al., 2017)).
592 **B.** Schematic of the chamber used for fission yeast. Left: design and dimensions (schematic not to
593 scale). Right: pillars are 60 µm in diameter and separated by 180 µm. **C.** Image of fission yeast cells in
594 an FXm experiment (prior to image normalization).

595

596 **Figure 2. Measuring fission yeast cell volume by FXm.** *A-D*, graphs are histograms with box and
597 whiskers plots, indicating the min, Q1, Q3 and max, with outliers determined by 1.5 IQR (interquartile
598 range). White dot indicates the median volume. Median volumes with s.d. are shown. **A.** Measurements
599 of wild-type fission yeast in five independent experiments (grey) and the total pooled dataset (black).
600 Chamber height: 5.53 µm; $n \geq 316$ for each replicate, $n=2266$ for the total dataset; values outside of the
601 plot range (n^*) were excluded: $n^* \leq 1$ for each replicate. **B.** Measurements of wild-type cells from a
602 single culture using five distinct devices of the indicated heights (grey) and the total pooled dataset
603 (black). $n \geq 225$ for each replicate, $n=1777$ for the total dataset; $n^*=0$ for each replicate. **C.** Top: wild
604 type (WT), *wee1-50*^{ts} and *cdc25-22*^{ts} temperature-sensitive strains were grown at the permissive
605 temperature of 25 °C and their volumes measured by FXm. Pooled datasets ($n \geq 1144$) of three
606 independent experiments ($n \geq 337$ for each replicate, Fig. S1A) are shown. $n^* \leq 6$ for each replicate.
607 Bottom: blankophor images with cell length at division (averages with s.d. for pooled datasets of three
608 independent experiments, $n \geq 100$ for each replicate). Scale bars = 10 µm. At 25 °C, WT cells have a
609 reduced volume and cell length at division compared to 32 °C (see *A*, *B* and Figs. 4-7). **D.** Top:
610 comparison of volume distributions in populations of WT haploid and diploid fission yeast cells by
611 FXm. Cells were grown in supplemented EMM6S at 32 °C. Pooled datasets ($n \geq 1073$) for three
612 independent experiments ($n \geq 207$ for each replicate, Fig. S1B) are shown. $n^* \leq 1$ for each replicate.
613 Bottom: blankophor images with cell length at division of the corresponding strains (averages with s.d.
614 for pooled datasets of three independent experiments, $n \geq 100$ for each replicate). Scale bars = 10 µm. In
615 EMM6S, WT cells have a volume that is similar to that in EMM (compare with *A*, *B* and Figs. 4-7) but
616 a reduced cell length at division (compare with Fig. 4A, 5A and 7), suggesting a difference in cell width
617 between these conditions.

618

619 **Figure 3. Analysis pipeline for FXm data. A.** Top: representative image showing the selection of
620 individual cells using the original FXm analysis code. Each cell must be identified from the FITC image

621 (see Fig. 1C; the area shown has been magnified for display purposes) and manually selected. Bottom:
622 representative image showing the tool that we developed, taking advantage of the normalization mask
623 for cell selection. All objects are automatically identified and displayed at a higher magnification. Cell
624 aggregates (bottom left), recently-divided cells (bottom right) or artifacts can be excluded by the user
625 (red-barred). **B.** Comparison of FXm results using manual (black) *vs.* automated (grey, 2 s.d. filter) cell
626 selection. Data for manual selection are from Fig. 2C. For automated selection, 1) the same images as
627 for the manual method were used, pooling the data from all replicates, and 2) a filter was applied that
628 excludes entries that are 2 s.d. above and below Q3 and Q1 (n^{**}), respectively (unfiltered selected
629 objects: $n \geq 1390$, excluded objects $n^{**} \leq 200$). The overlap between the two approaches for both correctly
630 assigned cells and outliers is between 87 and 92 %. Graphs are as in Fig. 2.

631

632 **Figure 4. FXm allows for the detection of subtle changes in cell volume and size distribution. A.**
633 Top: volume measurement of WT, MCN and MCN-AF cells by FXm. Pooled datasets ($n \geq 913$) of three
634 independent experiments ($n \geq 172$ for each replicate – Fig. S2) are shown. $n^{*} \leq 1$ for each replicate.
635 Graphs are as in Fig. 2. Bottom: blankophor images with cell length at division of the corresponding
636 strains (averages with s.d. for pooled datasets of three independent experiments, $n \geq 100$ for each
637 replicate). Scale bars = 10 µm. **B.** Comparison of the median volumes for 5 independent replicates of
638 WT at 25 and 32 °C. Full datasets are in Fig. S3A. Difference in median cell volume: 8.8 %. **C**. MCN
639 cells grown in EMM6S at 32 °C were G2-arrested using 1 µM 3-MBPP1 for 160 min and allowed to
640 synchronously re-enter the cell cycle by washing off the inhibitor (Coudreuse and Nurse, 2010) (Fig.
641 S3B). Cells were then injected in a FXm chip, and images were acquired at 5 min intervals throughout
642 the next G2, after cells had undergone a first round of mitosis and cell division (60 min, Fig. S3C). Top:
643 median population volumes at the indicated time points (black line – automated cell selection) with IQR
644 (grey area) are shown. Note that the higher volume for MCN cells compared to other Figures results
645 from the initial G2 block, during which cells grow without dividing. The phases of the cell cycle during
646 which cell volume was measured (first G2 and mitosis/M after release – Fig. S3C) are indicated. G2
647 growth rate: 0.59 $\mu m^3.min^{-1}$ (linear regression from 60 to 110 min, prior to the mitotic plateau). From
648 125 to 140 min, the automated selection does not separate newly divided cells (17.4%, 25.9% and 25.5%
649 of the selected objects at 130, 135 and 140 min, respectively, are pairs of cells; the remainder of the
650 cells have not undergone cytokinesis at these time points). This results in an apparent increased growth
651 rate. Note the delay in cell cycle progression compared to Fig. S3C, which may be due to the growth
652 conditions in the absence of medium flow (see Fig. 8B). For each time point, $214 \leq n \leq 278$ (unfiltered
653 automatically selected objects). Outliers were removed using the 2 s.d. filter (see Fig. 3B; $28 \leq n^{**} \leq 49$,
654 representing a maximum of 18% of the number of selected objects). Bottom: representative images for
655 cells in FXm chips at 85 min (G2), 120 min (M) and 135 min (pairs of sister cells represent a significant

656 subset of the population at this time point, see above). **D.** Volume distribution for the indicated strains
657 as a percentage of the median volume of the population. Data are as in *A*. $n^*\leq 10$.

658

659 **Figure 5. Measuring the volume of yeast cells with altered morphologies. A, C, E.** Blankophor
660 images with cell length at division of the indicated strains (averages with s.d. for pooled datasets of
661 three independent experiments, $n\geq 100$ for each replicate). n.d.: not determined. Scale bars = 10 µm. **B.**
662 Volume measurement by FXm of the strains in *A*. Pooled datasets ($n\geq 832$) of three independent
663 experiments ($n\geq 268$ for each replicate – Fig. S4) are shown. $n^*\leq 1$ for each replicate. **D.** Volume
664 measurement by FXm of the strains in *C*. Pooled datasets ($n\geq 940$) of three independent experiments
665 ($n\geq 230$ for each replicate – Fig. S5) are shown. $n^*=0$ for each replicate. Data for WT are as in Fig. 2D
666 (haploids). **E.** Blankophor images of WT cells in exponential growth and quiescence. For quiescent
667 cells, samples were taken 24 h after the culture reached OD_{595} 0.4. For proliferating cells, cell length at
668 division is shown (average with s.d. for pooled dataset of three independent experiments, $n\geq 100$ for
669 each replicate). n.d.: not determined. Scale bars = 10 µm. **F.** Volume measurement by FXm of the cells
670 in *E*. Pooled datasets ($n\geq 965$) of three independent experiments ($n\geq 238$ for each replicate – Fig. S6) are
671 shown. $n^*=0$ for each replicate. *C*, *D*: Experiments were carried out in EMM6S due to the presence of
672 auxotrophies in some of the strains (Table S2). *B, D, F:* Graphs are as in Fig. 2.

673

674 **Figure 6. FXm is compatible with the use of fluorescent markers to study subpopulations. A.** Top:
675 volume measurement of WT and cells expressing *nhp6::mCherry* by FXm. Pooled datasets ($n\geq 1568$)
676 of three independent experiments ($n\geq 499$ for each replicate – Fig. S7B) are shown. $n^*=0$ for each
677 replicate. Median volume values with s.d. are shown. Bottom: blankophor images with cell length at
678 division of the strains above (averages with s.d. for pooled datasets of three independent experiments,
679 $n\geq 110$ for each replicate). Scale bars = 10 µm. **B.** Volume comparison between mono- (grey) and bi-
680 nucleated (black) cells in the population of *nhp6::mCherry* cells as in *A*. The percentages and median
681 volumes for the mono- ($n=1619$) and binucleated ($n=196$) subpopulations are indicated. Binucleated
682 cells include both septated (dashed line) and non-septated cells. *A*, *B*: Graphs are as in Fig. 2.

683

684 **Figure 7. Dynamic changes in cell volume at the population level.** Left: FXm volume measurement
685 of MCN cells after treatment with 0.05 µM 3-MBPP1. Untreated WT cells were used as a control. For
686 MCN, samples were collected every 40 min after addition of the inhibitor ($n\geq 265$ at each time point,
687 $n=528$ for WT). $n^*\leq 2$ for each dataset. Graphs are as in Fig. 2. Right: blankophor images with average
688 cell length at division and s.d. for the experiment in *A*. $n\geq 100$ for WT and MCN (0, 120 and 160 min).
689 For the 40 and 80 min time points, the initial delay in mitosis due to the inhibitor treatment leads to a
690 reduction in the number of dividing cells, making it difficult to obtain similar numbers for the

691 calculation of cell length at division (*n*=45 and 22, respectively). Septation indices: WT: 11.5 %, MCN
692 0 min: 20.4 %, MCN 40 min: 1 %, MCN 80 min: 2 %, MCN 120 min: 15.5 %, MCN 160 min: 26.9 %;
693 *n*≥400 for each time point. Scale bars = 10 µm.

694

695 **Figure 8. Determination and real-time monitoring of single-cell volume by FXm. A.** 20 consecutive
696 FXm images were acquired (see Materials and Methods; 100 ms exposure per image over a total time
697 of 6 s) and the volumes of 10 individual cells were followed throughout the experiment. The generation
698 time of WT cells in these conditions is ~140 min. The coefficients of variation are between 0.3 and
699 3.1%. **B.** FXm time-lapse experiment using WT in EMM at 32 °C without medium flow. **C.** FXm time-
700 lapse experiment using WT in EMM at 32 °C with a constant flow of medium (3-5 $\mu L.min^{-1}$) containing
701 FITC-Dextran. *B*, *C*: individual traces represent the volume dynamics of single-cell lineages (at each
702 division, only one of the two daughter cells is further monitored). Volumes were determined every 10
703 min. For display purposes, the traces are aligned to the first division (see Materials and Methods).
704 Average growth rates with s.d. are shown for each cycle. Note that the growth rate in *C* is consistent to
705 that obtained from the bulk analysis of a synchronized population (Fig. 4C).

706

707 **REFERENCES**

708 **Amodeo, A. A. and Skotheim, J. M.** (2016). Cell-Size Control. *Cold Spring Harb Perspect Biol* **8**,
709 a019083.

710 **Baybay, E. K., Esposito, E. and Hauf, S.** (2020). Pomegranate: 2D segmentation and 3D
711 reconstruction for fission yeast and other radially symmetric cells. *Scientific reports* **10**, 16580–
712 15.

713 **Beinhauer, J. D., Hagan, I. M., Hegemann, J. H. and Fleig, U.** (1997). Mal3, the fission yeast
714 homologue of the human APC-interacting protein EB-1 is required for microtubule integrity and
715 the maintenance of cell form. *The Journal of cell biology* **139**, 717–728.

716 **Bishop, A. C., Ubersax, J. A., Petsch, D. T., Matheos, D. P., Gray, N. S., Blethrow, J., Shimizu,**
717 **E., Tsien, J. Z., Schultz, P. G., Rose, M. D., et al.** (2000). A chemical switch for inhibitor-
718 sensitive alleles of any protein kinase. *Nature* **407**, 395–401.

719 **Bryan, A. K., Goranov, A., Amon, A. and Manalis, S. R.** (2010). Measurement of mass, density,
720 and volume during the cell cycle of yeast. *Proc. Natl. Acad. Sci. U.S.A.* **107**, 999–1004.

721 **Bryan, A. K., Hecht, V. C., Shen, W., Payer, K., Grover, W. H. and Manalis, S. R.** (2014).
722 Measuring single cell mass, volume, and density with dual suspended microchannel resonators.
723 *Lab Chip* **14**, 569–576.

724 **Cadart, C., Monnier, S., Grilli, J., Sáez, P. J., Srivastava, N., Attia, R., Terriac, E., Baum, B.,**
725 **Cosentino-Lagomarsino, M. and Piel, M.** (2018). Size control in mammalian cells involves
726 modulation of both growth rate and cell cycle duration. *Nat Commun* **9**, 3275–15.

Cadart, C., Venkova, L., Recho, P., Lagomarsino, M. C. and Piel, M. (2019). The physics of cell-size regulation across timescales. *Nat. Phys.* **15**, 993–1004.

Cadart, C., Zlotek-Zlotkiewicz, E., Venkova, L., Thouvenin, O., Racine, V., Le Berre, M., Monnier, S. and Piel, M. (2017). Fluorescence eXclusion Measurement of volume in live cells. *Methods Cell Biol.* **139**, 103–120.

Chen, T., Gómez-Escoda, B., Munoz-Garcia, J., Babic, J., Griscom, L., Wu, P.-Y. J. and Coudreuse, D. (2016). A drug-compatible and temperature-controlled microfluidic device for live-cell imaging. *Open Biol* **6**, 160156.

Cook, M. and Tyers, M. (2007). Size control goes global. *Curr. Opin. Biotechnol.* **18**, 341–350.

Coudreuse, D. and Nurse, P. (2010). Driving the cell cycle with a minimal CDK control network. *Nature* **468**, 1074–1079.

Das, M., Wiley, D. J., Medina, S., Vincent, H. A., Larrea, M., Oriolo, A. and Verde, F. (2007). Regulation of cell diameter, For3p localization, and cell symmetry by fission yeast Rho-GAP Rga4p. *Molecular biology of the cell* **18**, 2090–2101.

Facchetti, G., Knapp, B., Flor-Parra, I., Chang, F. and Howard, M. (2019). Reprogramming Cdr2-Dependent Geometry-Based Cell Size Control in Fission Yeast. *Current biology : CB* **29**, 350–358.e4.

Fantes, P. (1979). Epistatic gene interactions in the control of division in fission yeast. *Nature* **279**, 428–430.

Fantes, P. A. (1977). Control of cell size and cycle time in Schizosaccharomyces pombe. *J. Cell. Sci.* **24**, 51–67.

Fantes, P. A. and Nurse, P. (1978). Control of the timing of cell division in fission yeast. Cell size mutants reveal a second control pathway. *Experimental cell research* **115**, 317–329.

Fantes, P. and Nurse, P. (1977). Control of cell size at division in fission yeast by a growth-modulated size control over nuclear division. *Experimental cell research* **107**, 377–386.

Grant, N. A., Abdel Magid, A., Franklin, J., Dufour, Y. and Lenski, R. E. (2021). Changes in Cell Size and Shape during 50,000 Generations of Experimental Evolution with Escherichia coli. *Journal of bacteriology* **203**.

Hayles, J. and Nurse, P. (1992). Genetics of the fission yeast Schizosaccharomyces pombe. *Annu. Rev. Genet.* **26**, 373–402.

Jeffares, D. C., Rallis, C., Rieux, A., Speed, D., Převorovský, M., Mourier, T., Marsellach, F. X., Iqbal, Z., Lau, W., Cheng, T. M. K., et al. (2015). The genomic and phenotypic diversity of Schizosaccharomyces pombe. *Nature genetics* **47**, 235–241.

Lancaster, O. M., Le Berre, M., Dimitracopoulos, A., Bonazzi, D., Zlotek-Zlotkiewicz, E., Picone, R., Duke, T., Piel, M. and Baum, B. (2013). Mitotic rounding alters cell geometry to ensure efficient bipolar spindle formation. *Dev. Cell* **25**, 270–283.

Lenski, R. E. and Travisano, M. (1994). Dynamics of adaptation and diversification: a 10,000-generation experiment with bacterial populations. *Proc. Natl. Acad. Sci. U.S.A.* **91**, 6808–6814.

765 **Li, Q., Rycaj, K., Chen, X. and Tang, D. G.** (2015). Cancer stem cells and cell size: A causal link?
766 *Semin. Cancer Biol.* **35**, 191–199.

767 **Lloyd, A. C.** (2013). The regulation of cell size. *Cell* **154**, 1194–1205.

768 **Marshall, W. F., Young, K. D., Swaffer, M., Wood, E., Nurse, P., Kimura, A., Frankel, J.,**
769 **Wallingford, J., Walbot, V., Qu, X., et al.** (2012). What determines cell size? *BMC Biol.* **10**,
770 101.

771 **Martin, S. G. and Berthelot-Grosjean, M.** (2009). Polar gradients of the DYRK-family kinase
772 Pom1 couple cell length with the cell cycle. *Nature* **459**, 852–856.

773 **Mata, J. and Nurse, P.** (1997). tea1 and the microtubular cytoskeleton are important for generating
774 global spatial order within the fission yeast cell. *Cell* **89**, 939–949.

775 **McDonald, J. C. and Whitesides, G. M.** (2002). Poly(dimethylsiloxane) as a material for fabricating
776 microfluidic devices. *Acc. Chem. Res.* **35**, 491–499.

777 **Millar, J. B., Buck, V. and Wilkinson, M. G.** (1995). Pyp1 and Pyp2 PTPases dephosphorylate an
778 osmosensing MAP kinase controlling cell size at division in fission yeast. *Genes & development*
779 **9**, 2117–2130.

780 **Mitchison, J. M.** (1957). The growth of single cells. I. Schizosaccharomyces pombe. *Experimental*
781 *cell research* **13**, 244–262.

782 **Mitchison, J. M. and Nurse, P.** (1985). Growth in cell length in the fission yeast
783 Schizosaccharomyces pombe. *J. Cell. Sci.* **75**, 357–376.

784 **Model, M.** (2020). Comparison of cell volume measurements by fluorescence and absorption
785 exclusion microscopy. *J Microsc* **280**, 12–18.

786 **Model, M. A.** (2018). Methods for cell volume measurement. *Cytometry A* **93**, 281–296.

787 **Mongold, J. A. and Lenski, R. E.** (1996). Experimental rejection of a nonadaptive explanation for
788 increased cell size in Escherichia coli. *Journal of bacteriology* **178**, 5333–5334.

789 **Moreno, S., Klar, A. and Nurse, P.** (1991). Molecular genetic analysis of fission yeast
790 Schizosaccharomyces pombe. *Meth. Enzymol.* **194**, 795–823.

791 **Moseley, J. B., Mayeux, A., Paoletti, A. and Nurse, P.** (2009). A spatial gradient coordinates cell
792 size and mitotic entry in fission yeast. *Nature* **459**, 857–860.

793 **Mueller, R. L.** (2015). Genome Biology and the Evolution of Cell-Size Diversity. *Cold Spring Harb*
794 *Perspect Biol* **7**, a019125.

795 **Navarro, F. J. and Nurse, P.** (2012). A systematic screen reveals new elements acting at the G2/M
796 cell cycle control. *Genome Biol.* **13**, R36.

797 **Nurse, P.** (1975). Genetic control of cell size at cell division in yeast. *Nature* **256**, 547–551.

798 **Pan, K. Z., Saunders, T. E., Flor-Parra, I., Howard, M. and Chang, F.** (2014a). Cortical
799 regulation of cell size by a sizer cdr2p. *Elife* **3**, e02040.

800 **Pan, K. Z., Saunders, T. E., Flor-Parra, I., Howard, M. and Chang, F.** (2014b). Cortical
801 regulation of cell size by a sizer cdr2p. *Elife* **3**, e02040.

802 **Pedersen, S. F., Hoffmann, E. K. and Mills, J. W.** (2001). The cytoskeleton and cell volume
803 regulation. *Comp. Biochem. Physiol., Part A Mol. Integr. Physiol.* **130**, 385–399.

804 **Petersen, J.** (2009). TOR signalling regulates mitotic commitment through stress-activated MAPK
805 and Polo kinase in response to nutrient stress. *Biochem. Soc. Trans.* **37**, 273–277.

806 **Pietras, A.** (2011). Cancer stem cells in tumor heterogeneity. *Adv. Cancer Res.* **112**, 255–281.

807 **Revilla-Guarinos, M. T., Martín-García, R., Villar-Tajadura, M. A., Estravís, M., Coll, P. M.**
808 **and Pérez, P.** (2016). Rga6 is a Fission Yeast Rho GAP Involved in Cdc42 Regulation of
809 Polarized Growth. *Molecular biology of the cell*.

810 **Saunders, T. E., Pan, K. Z., Angel, A., Guan, Y., Shah, J. V., Howard, M. and Chang, F.** (2012).
811 Noise reduction in the intracellular pom1p gradient by a dynamic clustering mechanism. *Dev.*
812 *Cell* **22**, 558–572.

813 **Scheffler, K., Recouvreux, P., Paoletti, A. and Tran, P. T.** (2014). Oscillatory AAA+ ATPase
814 Knk1 constitutes a novel morphogenetic pathway in fission yeast. *Proc. Natl. Acad. Sci. U.S.A.*
815 **111**, 17899–17904.

816 **Soifer, I., Robert, L. and Amir, A.** (2016). Single-Cell Analysis of Growth in Budding Yeast and
817 Bacteria Reveals a Common Size Regulation Strategy. *Current biology : CB* **26**, 356–361.

818 **Soto, T., Villar-Tajadura, M. A., Madrid, M., Vicente, J., Gacto, M., Pérez, P. and Cansado, J.**
819 (2010). Rga4 modulates the activity of the fission yeast cell integrity MAPK pathway by acting
820 as a Rho2 GTPase-activating protein. *The Journal of biological chemistry* **285**, 11516–11525.

821 **Sun, S. and Gresham, D.** (2021). Cellular quiescence in budding yeast. *Yeast* **38**, 12–29.

822 **Sveiczer, A., Novak, B. and Mitchison, J. M.** (1996). The size control of fission yeast revisited. *J.*
823 *Cell. Sci.* **109 (Pt 12)**, 2947–2957.

824 **Taheri-Araghi, S., Bradde, S., Sauls, J. T., Hill, N. S., Levin, P. A., Paulsson, J., Vergassola, M.**
825 **and Jun, S.** (2015). Cell-size control and homeostasis in bacteria. *Current biology : CB* **25**, 385–
826 391.

827 **Villar-Tajadura, M. A., Coll, P. M., Madrid, M., Cansado, J., Santos, B. and Pérez, P.** (2008).
828 Rga2 is a Rho2 GAP that regulates morphogenesis and cell integrity in S. pombe. *Mol.*
829 *Microbiol.* **70**, 867–881.

830 **Vjestica, A., Zhang, D., Liu, J. and Oliferenko, S.** (2013). Hsp70-Hsp40 chaperone complex
831 functions in controlling polarized growth by repressing Hsf1-driven heat stress-associated
832 transcription. *PLOS Genetics* **9**, e1003886.

833 **Yang, J., Dungrawala, H., Hua, H., Manukyan, A., Abraham, L., Lane, W., Mead, H., Wright,**
834 **J. and Schneider, B. L.** (2011). Cell size and growth rate are major determinants of replicative
835 lifespan. *Cell cycle* **10**, 144–155.

836 **Zegman, Y., Bonazzi, D. and Minc, N.** (2015). Measurement and manipulation of cell size
837 parameters in fission yeast. *Methods Cell Biol.* **125**, 423–436.

838 **Zhurinsky, J., Leonhard, K., Watt, S., Marguerat, S., Bähler, J. and Nurse, P.** (2010). A
839 coordinated global control over cellular transcription. *Current biology : CB* **20**, 2010–2015.

Zlotek-Zlotkiewicz, E., Monnier, S., Cappello, G., Le Berre, M. and Piel, M. (2015). Optical volume and mass measurements show that mammalian cells swell during mitosis. *The Journal of cell biology* **211**, 765–774.

FIGURE 1

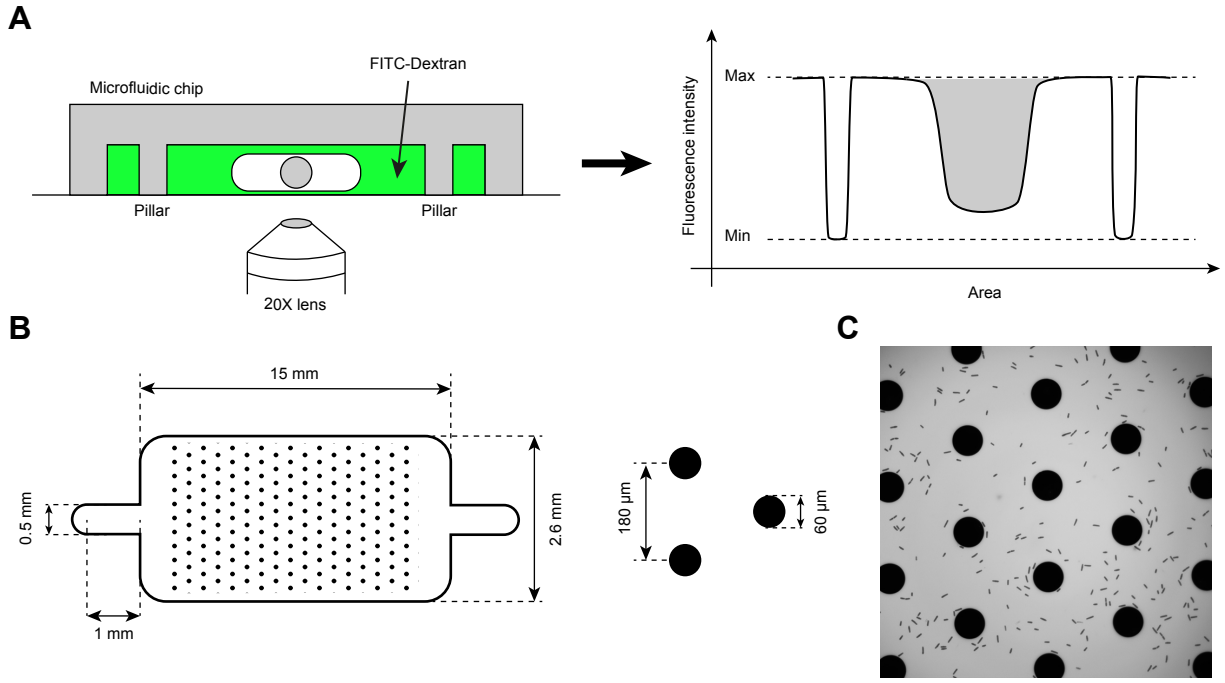
A
Microfluidic chip
FITC-Dextran
Pillar
Pillar
20X lens
Fluorescence intensity
Max
Min
Area
B
15 mm
0.5 mm
2.6 mm
1 mm
180 µm
60 µm
C

FIGURE 2

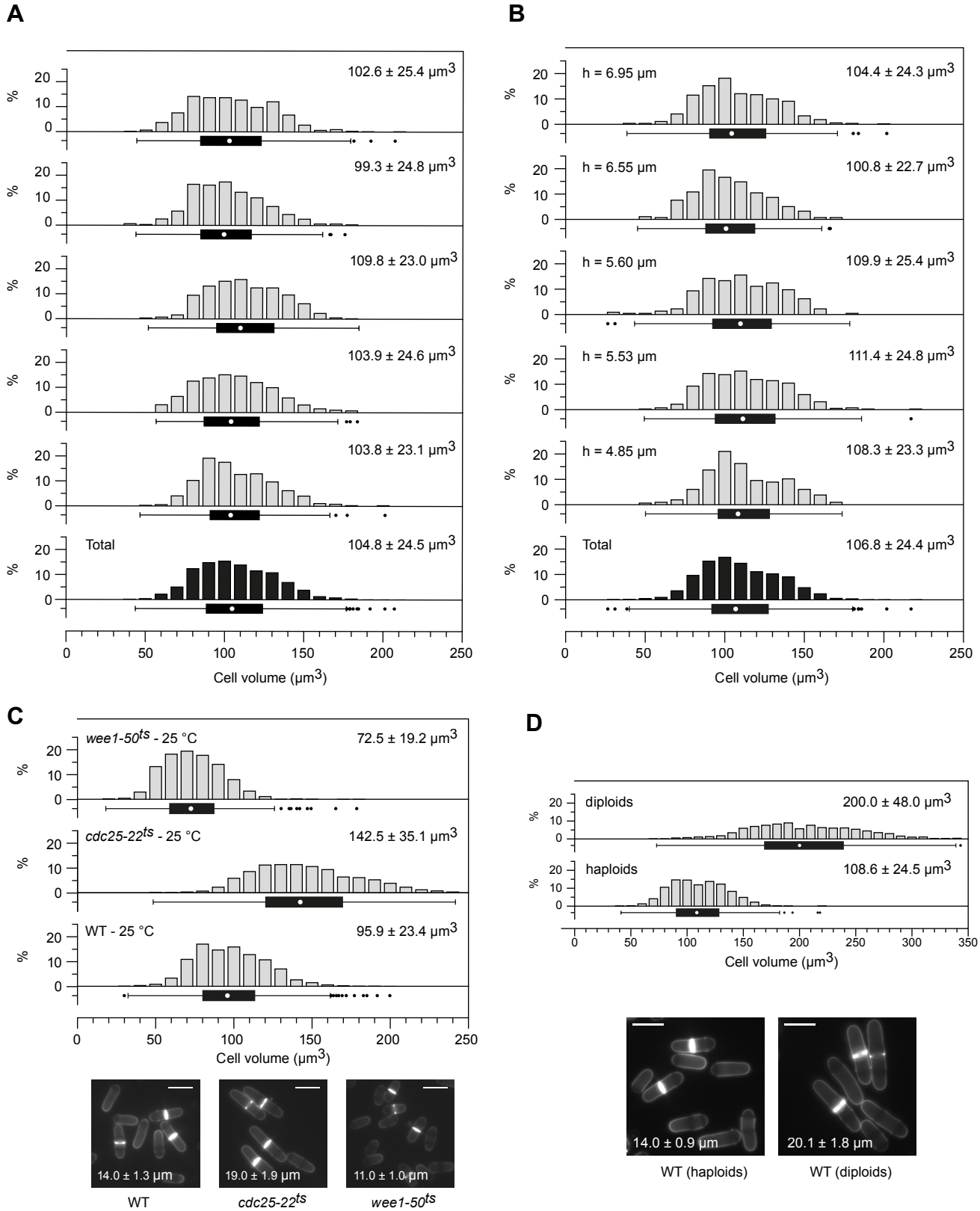
A
102.6 ± 25.4 µm3
99.3 ± 24.8 µm3
109.8 ± 23.0 µm3
103.9 ± 24.6 µm3
103.8 ± 23.1 µm3
Total
104.8 ± 24.5 µm3
Cell volume (µm3)
B
h = 6.95 µm
104.4 ± 24.3 µm3
h = 6.55 µm
100.8 ± 22.7 µm3
h = 5.60 µm
109.9 ± 25.4 µm3
h = 5.53 µm
111.4 ± 24.8 µm3
h = 4.85 µm
108.3 ± 23.3 µm3
Total
106.8 ± 24.4 µm3
Cell volume (µm3)
C
wee1-50ts - 25 °C
72.5 ± 19.2 µm3
cdc25-22ts - 25 °C
142.5 ± 35.1 µm3
WT - 25 °C
95.9 ± 23.4 µm3
Cell volume (µm3)
14.0 ± 1.3 µm
WT
19.0 ± 1.9 µm
cdc25-22ts
11.0 ± 1.0 µm
wee1-50ts
D
diploids
200.0 ± 48.0 µm3
haploids
108.6 ± 24.5 µm3
Cell volume (µm3)
14.0 ± 0.9 µm
WT (haploids)
20.1 ± 1.8 µm
WT (diploids)

FIGURE 3

A

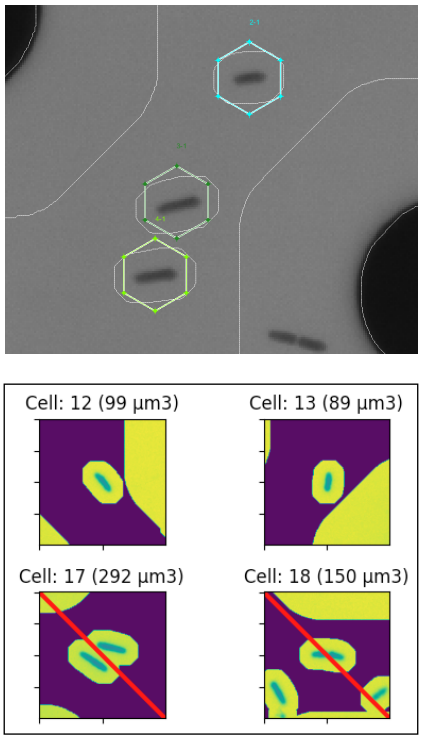
Cell: 12 (99 µm3)
Cell: 13 (89 µm3)
Cell: 17 (292 µm3)
Cell: 18 (150 µm3)

B

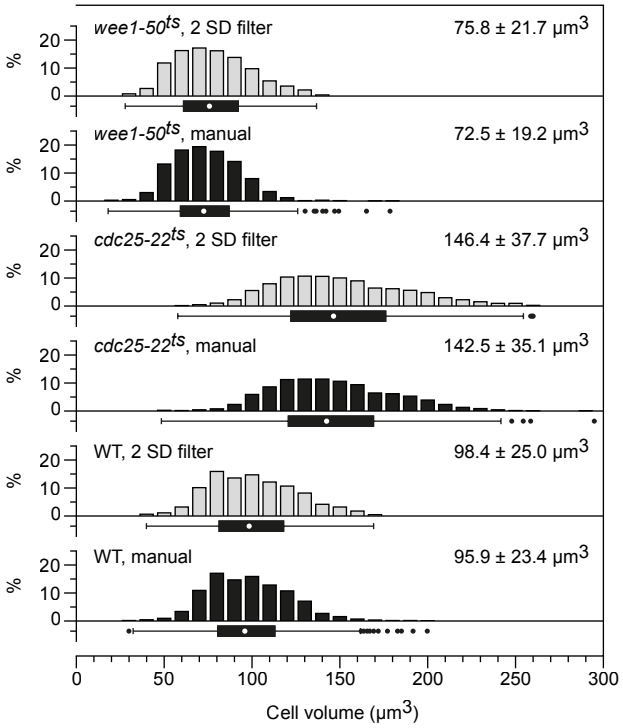
wee1-50ts, 2 SD filter
75.8 ± 21.7 µm3
wee1-50ts, manual
72.5 ± 19.2 µm3
cdc25-22ts, 2 SD filter
146.4 ± 37.7 µm3
cdc25-22ts, manual
142.5 ± 35.1 µm3
WT, 2 SD filter
98.4 ± 25.0 µm3
WT, manual
95.9 ± 23.4 µm3
%
0
10
20
0
50
100
150
200
250
300
Cell volume (µm3)

FIGURE 4

A

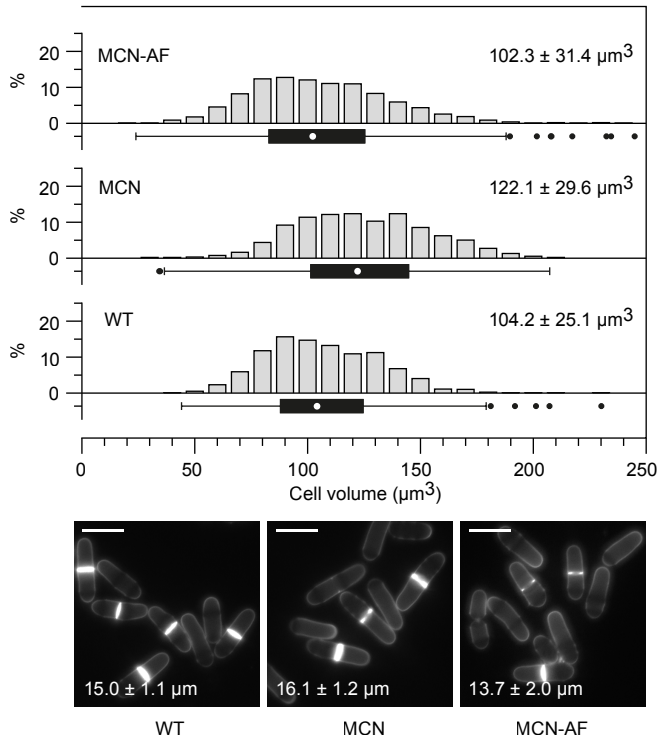

B

	25 °C	32 °C
	99.1 ± 21.8 µm^3	109.8 ± 23.0 µm^3
	97.8 ± 21.2 µm^3	103.9 ± 24.6 µm^3
	94.2 ± 20.4 µm^3	103.8 ± 23.1 µm^3
	93.6 ± 23.7 µm^3	102.6 ± 25.4 µm^3
	93.3 ± 20.5 µm^3	99.3 ± 24.8 µm^3
Full datasets:	**96.3 ± 21.9 µm^3**	**104.8 ± 24.5 µm^3**

C

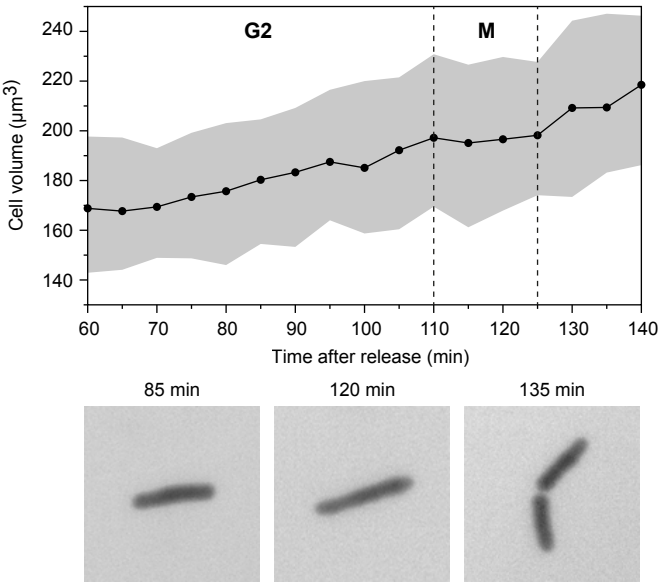

D

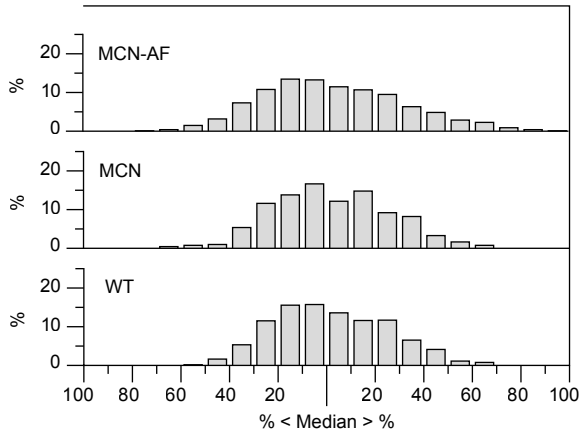

FIGURE 5

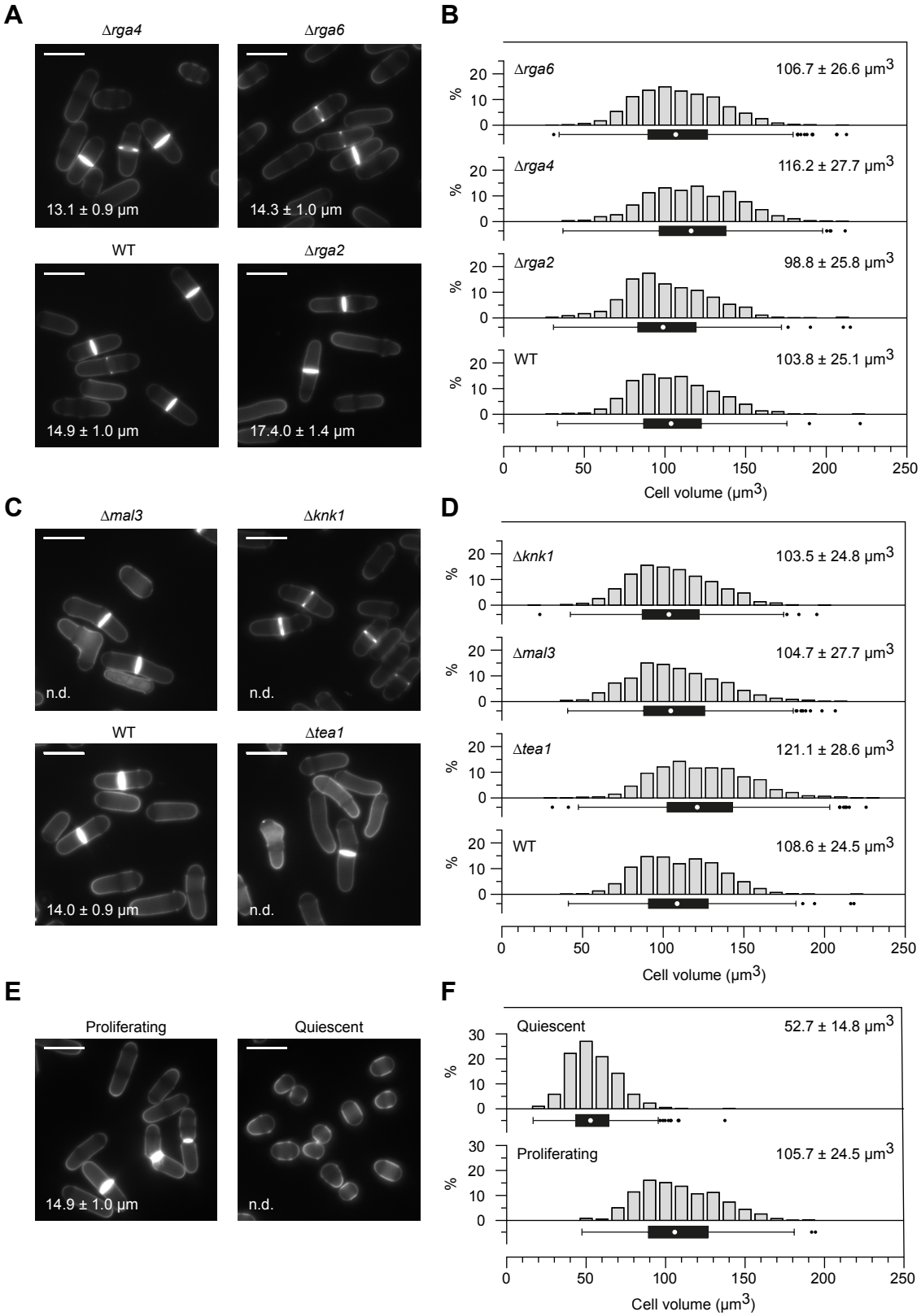
A
Δrga4
Δrga6
13.1 ± 0.9 µm
14.3 ± 1.0 µm
WT
Δrga2
14.9 ± 1.0 µm
17.4.0 ± 1.4 µm
B
Δrga6
106.7 ± 26.6 µm3
Δrga4
116.2 ± 27.7 µm3
Δrga2
98.8 ± 25.8 µm3
WT
103.8 ± 25.1 µm3
%
Cell volume (µm3)
C
Δmal3
Δknk1
n.d.
WT
Δtea1
14.0 ± 0.9 µm
D
Δknk1
103.5 ± 24.8 µm3
Δmal3
104.7 ± 27.7 µm3
Δtea1
121.1 ± 28.6 µm3
WT
108.6 ± 24.5 µm3
E
Proliferating
Quiescent
14.9 ± 1.0 µm
F
Quiescent
52.7 ± 14.8 µm3
Proliferating
105.7 ± 24.5 µm3

FIGURE 6

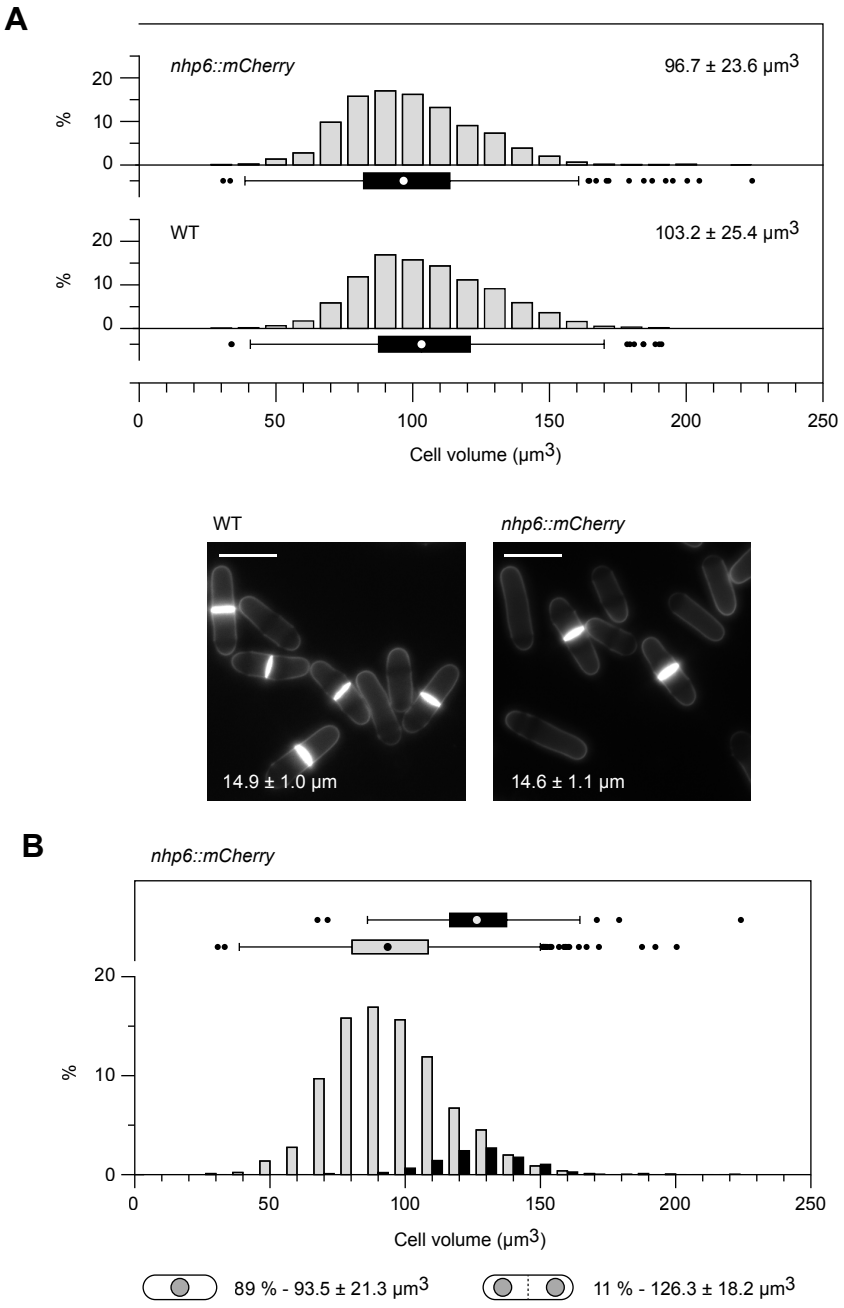
A
nhp6::mCherry
96.7 ± 23.6 µm3
WT
103.2 ± 25.4 µm3
%
20
10
0
0
50
100
150
200
250
Cell volume (µm3)
WT
nhp6::mCherry
14.9 ± 1.0 µm
14.6 ± 1.1 µm
B
nhp6::mCherry
89 % - 93.5 ± 21.3 µm3
11 % - 126.3 ± 18.2 µm3

FIGURE 7

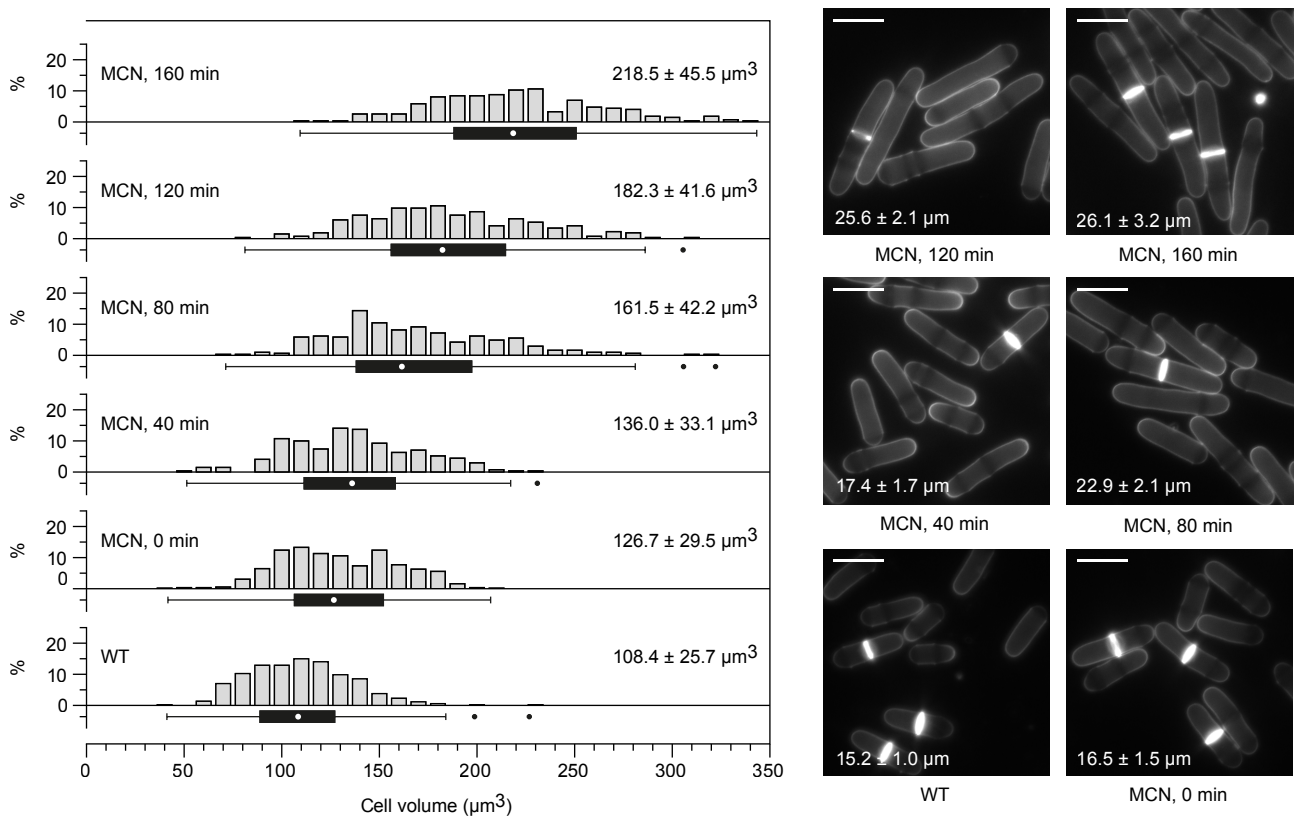
MCN, 160 min
218.5 ± 45.5 μm3
MCN, 120 min
182.3 ± 41.6 μm3
MCN, 80 min
161.5 ± 42.2 μm3
MCN, 40 min
136.0 ± 33.1 μm3
MCN, 0 min
126.7 ± 29.5 μm3
WT
108.4 ± 25.7 μm3
%
Cell volume (μm3)
25.6 ± 2.1 μm
MCN, 120 min
26.1 ± 3.2 μm
MCN, 160 min
17.4 ± 1.7 μm
MCN, 40 min
22.9 ± 2.1 μm
MCN, 80 min
15.2 ± 1.0 μm
WT
16.5 ± 1.5 μm
MCN, 0 min

FIGURE 8

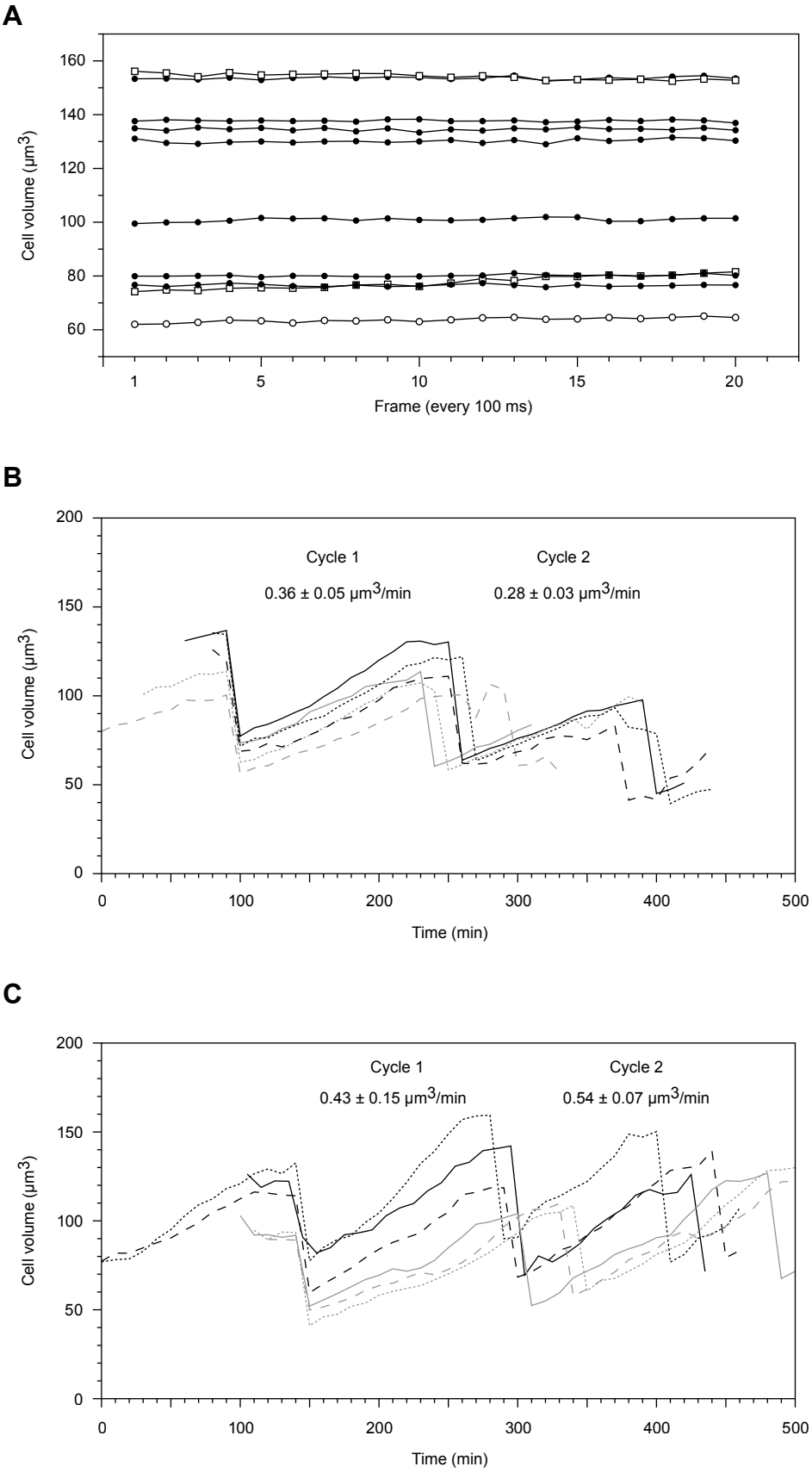
A
Cell volume (µm3)
160
140
120
100
80
60
1
5
10
15
20
Frame (every 100 ms)
B
Cell volume (µm3)
200
150
100
50
0
Cycle 1
0.36 ± 0.05 µm3/min
Cycle 2
0.28 ± 0.03 µm3/min
0
100
200
300
400
500
Time (min)
C
Cell volume (µm3)
200
150
100
50
0
Cycle 1
0.43 ± 0.15 µm3/min
Cycle 2
0.54 ± 0.07 µm3/min
0
100
200
300
400
500
Time (min)